Chemical Engineering Science 251 (2022) 117477

Contents lists available at ScienceDirect

Chemical Engineering Science

journal homepage: www.elsevier.com/locate/ces

Investigation of hydrogenation and mass transfer performance in micropacked beds with highly active monolithic catalysts

Chi Ma, Mengmeng Huang, Jiabin Yin, Fengyan Lou, Jisong Zhang *

State Key Laboratory of Chemical Engineering, Department of Chemical Engineering, Tsinghua University, Beijing 100084, China

HIGHLIGHTS

- The coatings prepared by slurry circulation had good uniformity.
- Active component Pd was uniformly distributed on the coatings.
- The activity of monolithic catalysts was higher than that of particle catalysts.
- The coatings had a certain influence on overall external mass transfer performance.

GRAPHICAL ABSTRACT

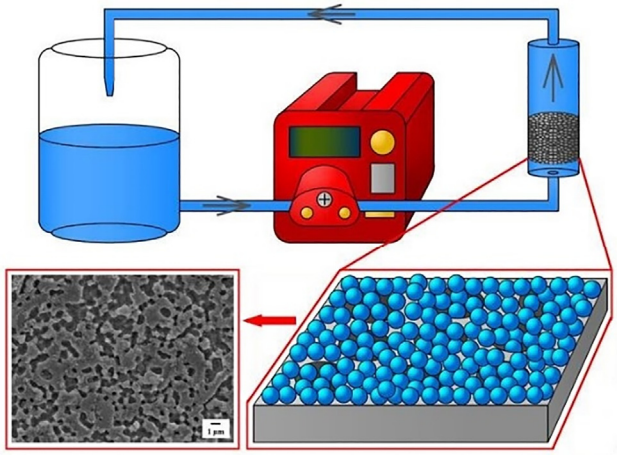

ARTICLE INFO

Article history:
Received 9 December 2021
Received in revised form 20 January 2022
Accepted 23 January 2022
Available online 29 January 2022

Keywords:
Monolithic catalyst
Nickel foam
Hydrogenation
Mass transfer
Micropacked bed

ABSTRACT

A method of slurry circulation for coating supports on nickel foams with small pore size is proposed to prepare monolithic catalysts used in micropacked beds (MPBs). Rather than the method applied to a single support material, this method is verified to be universal and applicable for various supports in this work. The coatings and active component Pd loaded on the coatings are demonstrated to be uniform. The coating weight can be predicted by an empirical correlation, revealing a law of coating weight. The monolithic catalysts exhibit high activity, long-term stability, and mechanical stability in the hydrogenation of α-methylstyrene. Moreover, the overall external mass transfer coefficient (k_{OV}) of catalysts is measured, showing that k_{OV} is affected by the properties of coatings. The catalysts prepared by slurry circulation method hopefully provide high activity and stability for various catalytic reactions in MPBs.

1. Introduction

Micropacked beds (MPBs) are derived from the miniaturization of trickle bed reactors (Losey et al., 2001; Cao et al., 2021), which have attracted substantial attentions (Nuzhdin et al., 2015; Vilé et al., 2015; Zhang et al., 2017). Compared with conventional trickle bed reactors, MPBs have the small dimensional scale and are packed with small particles (diameters < 500 μm) (Ranade et al., 2011; Zhang et al., 2018), which exhibit the advantages of high surface-to-volume ratio, enhanced mass transfer, fast multiphase mixing, and excellent operating safety (Liu et al., 2016; Zheng et al., 2019). At present, MPBs have been widely applied in

* Corresponding author.
E-mail address: jiszhang@tsinghua.edu.cn (J. Zhang).

https://doi.org/10.1016/j.ces.2022.117477
0009-2509/

Nomenclatures

a_c	intrinsic activity ($mol \cdot s^{-1} \cdot g_{Pd}^{-1}$)
C_{AMS}	AMS initial concentration (wt%)
$C^*_{H_2}$	hydrogen concentration at equilibrium ($mol \cdot m^{-3}$)
$C^l_{H_2}$	hydrogen concentration in the liquid ($mol \cdot m^{-3}$)
$C^s_{H_2}$	hydrogen concentration at catalyst surface ($mol \cdot m^{-3}$)
D_E	effective diffusivity ($m^2 \cdot s^{-1}$)
$D^l_{H_2}$	the molecular diffusivity in the liquid phase ($m^2 \cdot s^{-1}$)
d_p	pore size of nickel foam (m)
E_a	activation energy ($J \cdot mol^{-1}$)
G	gas flow rate ($mL \cdot min^{-1}$)
k_0	Arrhenius pre-exponential factor ($mol \cdot s^{-1} \cdot g_{Pd}^{-1}$)
k_{H_2}	hydrogen adsorption equilibrium constant ($m^3 \cdot mol^{-1}$)
k_{OV}	overall external mass transfer coefficient (s^{-1})
L_{cat}	catalyst layer thickness (m)
m_{Pd}	mass of active component Pd (g)
P	system pressure (MPa)
Q	liquid flow rate ($mL \cdot min^{-1}$)
Q_s	slurry flow rate ($mL \cdot min^{-1}$)
R	gas constant ($J \cdot mol^{-1} \cdot K^{-1}$)
r_a	apparent reaction rate ($mol \cdot s^{-1} \cdot g_{Pd}^{-1}$)
r_{int}	intrinsic reaction rate ($mol \cdot s^{-1} \cdot g_{Pd}^{-1}$)
S	specific surface area ($m^2 \cdot g^{-1}$)
T	reaction temperature (°C)
u_g	gas superficial velocity ($m \cdot s^{-1}$)
u_l	liquid superficial velocity ($m \cdot s^{-1}$)
V_{cat}	catalyst volume (m^3)
V_L	liquid volume (m^3)
W	coating weight ($g \cdot (g\ nickel\ foam)^{-1}$)

Greek symbols

η	effectiveness factor
μ	slurry viscosity (cP)
μ_g	gas viscosity (Pa·s)
μ_l	liquid viscosity (Pa·s)
ρ	powders density ($g \cdot cm^{-3}$)
ρ_g	gas density ($kg \cdot m^{-3}$)
ρ_l	liquid density ($kg \cdot m^{-3}$)
Φ	Thiele modulus
χ_{AMS}	AMS conversion

Dimensionless numbers

Re_g	gas Reynolds number $= \frac{\rho_g \cdot u_g \cdot d_p}{\mu_g}$
Re_l	liquid Reynolds number $= \frac{\rho_l \cdot u_l \cdot d_p}{\mu_l}$
Sc_l	liquid Schmidt number $= \frac{\mu_l}{\rho_l \cdot D^l_{H_2}}$

gas–liquid-solid reactions, such as hydrogenation (Kataoka et al., 2012; Feng et al., 2016) and oxidation (Cao et al., 2021; Shang et al., 2013; Shang et al., 2015). However, high pressure drop will be generated in the MPBs with such small particles, leading to a high energy consumption and operating cost (Sang et al., 2020).

Metal foam is a class of structural material, offering several features of high porosity, low pressure drop, interconnected pore structure, and attractive thermal and mechanical stability (Yu et al., 2007; Sang et al., 2012), which is regarded as the outstanding material for catalyst substrate (Wang et al., 2016; Sudhakaran et al., 2019; Wang et al., 2019). The combination of metal foam and catalyst particles is used to prepare monolithic catalysts in recent years. In addition, metal foam monolithic catalysts can promote active component dispersion, minimize sintering, and stabilize coke formation (Bobadilla et al., 2012; Koc and Avci, 2017; Chen et al., 2020). Therefore, it presents a flexible approach for the applications of metal foam monolithic catalysts in the MPBs, which hopefully reduce the pressure drop and intensify the catalytic performance in the meanwhile. Liang et al. (2017) investigated the Cu-Zn/Al foam monolithic catalyst in a microreactor, and the catalyst delivered a high yield of methanol in the CO_2 hydrogenation reaction. Wang et al. (2019) prepared a Ru-Ni/Ni foam monolithic catalyst for hydrogen production from $NaBH_4$, and the reaction activity energy was much lower than previously published $NaBH_4$ spontaneous methanolysis. Zhu et al. (2019) reported the discovery of a Ni_3P/Ni-foam monolithic catalyst, which was highly active and highly stable for the hydrogenation of dimethyl oxalate to methyl glycolate.

The reactions can be intensified by loading the active components onto the metal foams. However, the specific surface area of metal foams is relatively low, restricting the development of catalysts (Li et al., 2013; Jin and Kwon, 2009). An intermediate layer was needed to increase the specific surface area and further improve the catalyst properties (Wang et al., 2016). Many efforts have been devoted to fabricating the catalyst supports on metal foams for the monolithic catalysts. Roy et al. (2018) investigated variable $CeZrO_2$-Al_2O_3 support compositions on metal foam, and coated Pd-Rh catalysts for biogas conversion to syngas by steam reforming. Catalysts with a larger $CeZrO_2/Al_2O_3$ ratio exhibited higher CH_4 and CO_2 conversions, higher H_2/CH_4 yields, lower H_2/CO ratios, and reduced coke formation. Xue et al. (2021) developed a TiO_2 film on nickel foam and loaded $Zn_{0.95}Fe_{0.05}S$ as monolithic catalyst, which was induced into photocatalytic system. The catalyst showed a high utilization of supports, attributing to the integration of three independent materials.

One of the most common methods for preparing catalyst supports is coating by sol–gel slurry (Ma et al., 2019). Whereas, the pore size of metal foam used in MPBs is usually smaller than 500 μm for creating microchannels and cavities (Yang et al., 2018; Tu et al., 2020). The slurry is difficult to flow into the pores of metal foam because of the high capillary force, and the distribution of catalyst coatings is nonuniform when the slurry impregnation is used (Zheng et al., 2019). At present, there are few reports on how to fabricate uniformly distributed catalyst coatings and control the coating weight, which significantly affect the catalyst properties (Zanota et al., 2018). Moreover, the mass transfer performance of the MPBs with metal foam monolithic catalysts at such small pore size is still unclear.

Based on our previous work of sol–gel slurry method applied to a single support material (Ma et al., 2021), a universal and applicable method for the preparation of catalyst coatings was proposed in this work. Various coatings, including Al_2O_3, SiO_2, CeO_2, TiO_2, and $CaCO_3$ were applied on the metal foams, and an empirical correlation was established to predict the coating weight. The uniformity of the catalyst coatings was characterized, and the activity and stability of the catalysts were evaluated by α-methylstyrene (AMS) hydrogenation reaction in the MPB. The overall external mass transfer coefficient (k_{OV}) and correlation were also investigated for a better understanding of the gas–liquid-solid mass transfer process in MPBs.

2. Experimental section

2.1. Catalyst preparation and characterization

Nickel foam (Kunshan Jiayisheng Electronic Co., Ltd., China) with 130 pores per inch (PPI) was employed as catalyst substrate and cut into cylindrical pieces. The diameter and height of the

pieces were 3.8 mm and 5.0 mm, respectively. These nickel foams were firstly washed by deionized water (self-prepared) and alcohol for 30 min, respectively, in an ultrasonic cleaner (KQ5200DE, Kunshan Ultrasonic Instrument Co., Ltd., China) with the frequency of 40 kHz and power of 200 W. Then the nickel foams were pretreated by a mixed acid solution of HCl, HNO_3 (Beijing Lanyi Chemical Products, Co., Ltd., China), and deionized water. HCl: HNO_3: deionized water (volume ratio) of 3: 1: 15, etching time of 45 min, and etching temperature of 20 °C were chosen to improve the roughness of substrate surface. After pretreatment, the nickel foams were ultrasonically washed in deionized water for 30 min to remove the remaining acid solution.

Subsequently, the catalyst coatings were prepared by a sol–gel method. Al_2O_3 powders (Jiangsu Xianfeng Nanomaterials Technology Co., Ltd., China), SiO_2 powders (Shanghai Xiangtian Nanomaterials Co., Ltd., China), CeO_2 powders (Shanghai Puzhen Biological Technology Co., Ltd., China), TiO_2 powders (Bangrui New Material Technology Co., Ltd., China), and $CaCO_3$ powders (Jiangsu Xianfeng Nanomaterials Technology Co., Ltd., China) were separately used for the coatings. Polyvinyl alcohol (PVA, Beijing Anxinkang Technology Co., Ltd., China) and deionized water were mixed and magnetically stirred for 2 h at 85 °C to dissolve the PVA. The powders and HNO_3 were added into the PVA solution and continuously stirred for 2 h to obtain the slurry. The PVA and HNO_3 were used as binder and stabilizer, respectively, and the concentrations of Al_2O_3, PVA, HNO_3, and deionized water were 12.0, 1.8, 1.2, and 85.0 wt%, respectively. After that, the slurry was kept at room temperature (25 °C) for 24 h to make it stable.

To overcome capillary force, the slurry was coated on the surface of pretreated nickel foams by slurry circulation method. The nickel foams were packed right in a tube with the inner diameter of 3.8 mm. The slurry was pumped and circulated by a peristaltic pump (BT00-300 M, Baoding Lange Constant Flow Pump Co., Ltd., China) for 30 min. The slurry flow rate (Q_s) of 18, 54, 90, 126, 162, and 198 mL·min^{-1} was chosen for different coating weights. Then the nickel foams were retained in the tube with the air circulation for 10 min to remove the remaining slurry. After coating, the nickel foams were successively dried in air at room temperature for 24 h, at 120 °C for 6 h, and calcined in an oven at 600 °C for 2 h with ramping up at 5 °C·min^{-1}. The preparation of coatings can be referred to our previous work (Ma et al., 2021).

At last, the active component was loaded using a wet impregnation method. $PdCl_2$ (Beijing Balinwei Technology Co., Ltd., China) was dissolved in the HCl solution with the concentration of 0.1 mol·L^{-1}. The nickel foams with coatings were immersed in the above solution and treated at 60 °C for 3 h, and the content of Pd loaded for each sample was 0.00003 g. The samples were dried and calcined in an oven at 400 °C for 2 h with ramping up at 2 °C·min^{-1}, and then reduced in hydrogen at 300 °C for 2 h with ramping up at 5 °C·min^{-1}. After that, the monolithic catalysts were obtained, and the schematic diagram of the monolithic catalyst preparation process is shown in Fig. 1.

The surface morphologies of the samples were analyzed by a scanning electron microscope (SEM, Sirion200, FEI, Netherlands). The textural properties of the samples were determined at −196 °C by a dynamic nitrogen adsorption apparatus (Autosorb-1-C, Quantachrome Instruments, U.S.) with the samples pretreated at 200 °C for 6 h. The specific surface area was calculated by the Brunauer-Emmett-Teller (BET) method.

2.2. Catalyst performance test

The hydrogenation of AMS (Shanghai McLean Biochemical Technology Co., Ltd., China) to cumene was used as a model reaction for catalyst performance test. The schematic diagram of the experimental setup is shown in Fig. 2. The MPB was made of stainless steel, and the inner diameter, outer diameter, and length were 3.8, 6.4, and 80.0 mm, respectively. Four pieces of monolithic catalysts were packed in the middle of the MPB, and other parts of the MPB were packed with untreated nickel foams.

AMS dissolved in methanol (Shanghai Titan Technology Co., Ltd., China) was pumped and mixed with pure hydrogen from regulated cylinder, and then flowed into the MPB. The MPB was installed in a water bath to control the reaction temperature (T) at 70 °C, and a back pressure regulator was employed to control the system pressure (P) at 1.0 MPa. AMS initial concentration (C_{AMS}) and the gas flow rate (G) were set as 10 wt% and 20 mL·min^{-1}, respectively. The liquid flow rate (Q) of 0.05, 0.1, 0.2, 0.3, 0.4, and 0.5 mL·min^{-1} was chosen in the experiments. When the reaction was stable, the liquid samples from the outlet of MPB were collected, diluted, and then analyzed by a gas chromatography (GC, 8860, Agilent Technologies Co., Ltd., U.S.) with a flame ionization detector (FID) and a capillary column (HP-5, 30 m × 0.32 mm × 0.25 μm).

The same MPB packed with Pd/Al_2O_3 particle catalysts was employed in this work for the comparison of hydrogenation performance. The catalysts were prepared by loading active component Pd on Al_2O_3 particles with the same method in Section 2.1. The Pd concentration of catalysts was controlled as 0.3 wt%, and the catalysts with 0.04 g were used for the similar content of Pd as the monolithic catalysts. The diameter of Al_2O_3 particles was about 460 μm, by which the similar channels as the nickel foam can be created. The particle catalysts were also packed in the middle of MPB, and other parts of the MPB were packed with blank Al_2O_3 particles.

2.3. Mass transfer performance evaluation

The overall external mass transfer performance was measured by the hydrogenation of AMS in methylcyclohexane (Shanghai Meryer Chemical Technology Co., Ltd., China) with the same experimental setup as the catalyst performance test in Section 2.2. The mass transfer performance of MPB both packed with monolithic catalysts and particle catalysts was investigated. The reaction temperature, pressure, AMS initial concentration, and gas flow rate were set as 30 °C, 0.6 MPa, 10 wt%, and 20 mL·min^{-1}, respectively. The AMS hydrogenation is an extremely fast reaction and enables to reach a fully mass transfer limited regime even at moderate temperature and pressure (Meille et al., 2004; Lévêque et al., 2016). Assuming a plug flow model, the apparent rate of reaction (r_a) can be determined by an integration of a steady state mass balance over the whole catalysts (Tourvieille et al., 2013; Tourvieille et al., 2015). The apparent rate can be expressed in terms of the AMS conversion and the liquid flow rate, as shown in equation (1) (Haase et al., 2013; Sang et al., 2020).

$$r_a = \frac{Q \cdot C_{AMS} \cdot \chi_{AMS}}{m_{Pd}} \tag{1}$$

where χ_{AMS} and m_{Pd} refer to the AMS conversion and the mass of active component Pd, respectively. The k_{OV} can be measured through the hydrogen balance between the gas phase and the catalyst layer, which is given in equation (2).

$$k_{OV} \cdot \left(C^*_{H_2} - C^s_{H_2}\right) \cdot V_L = r_a \cdot m_{Pd} = \eta \cdot r_{int} \cdot m_{Pd} \tag{2}$$

where $C^*_{H_2}$, $C^s_{H_2}$, V_L, η, and r_{int} refer to the hydrogen concentration at equilibrium, the hydrogen concentration at catalyst surface, the liquid volume, the effectiveness factor, and the intrinsic reaction rate, respectively. According to Herskowitz et al. (1978), the equilibrium concentration of hydrogen in pure AMS is described in equation (3). Considering the higher solubility of hydrogen in diluted AMS (10 wt

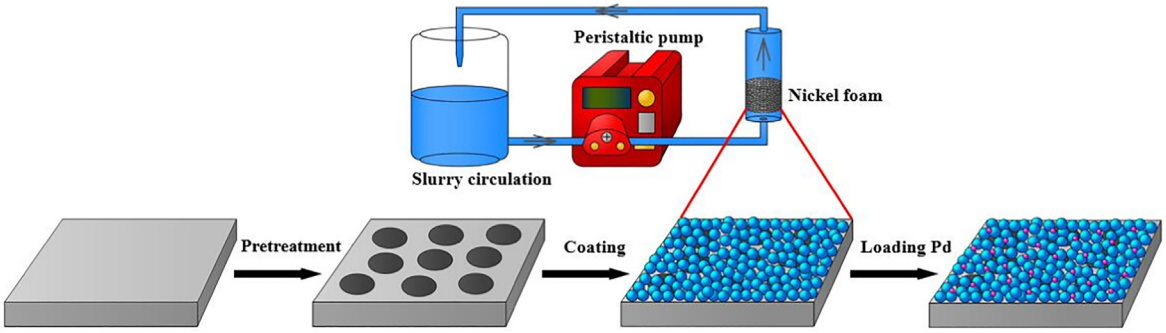

Fig. 1. Schematic diagram of monolithic catalyst preparation process.

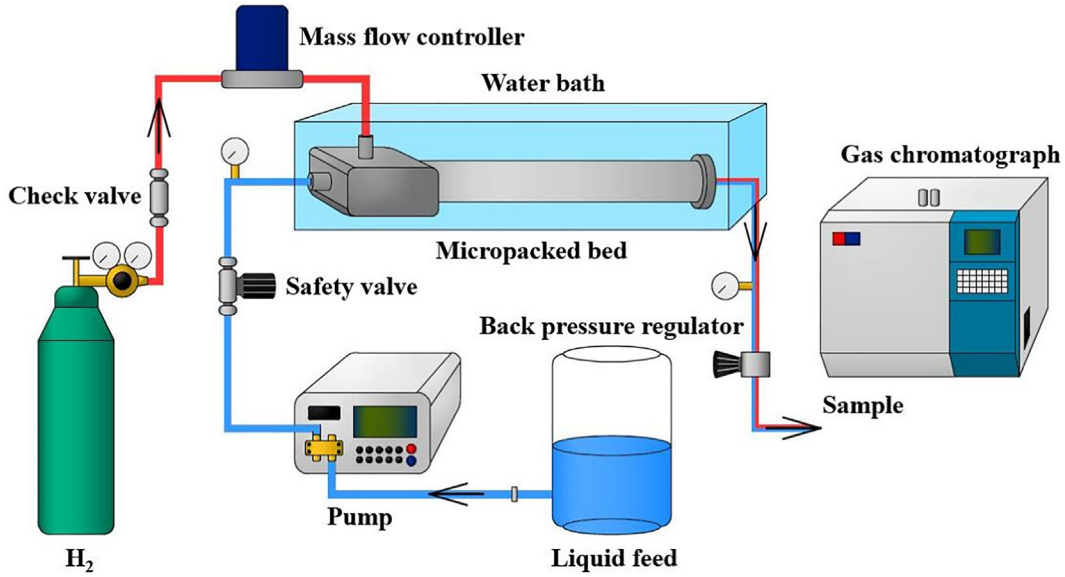

Fig. 2. Schematic diagram of the experimental setup for catalyst performance test.

% in methylcyclohexane) than that in pure AMS, a prefactor of 1.3 is required (Meille et al., 2002).

$$C^{*}_{H_2} = (0.0145T - 1.6985) \cdot P \tag{3}$$

To account for internal mass transfer limitation, the effectiveness factor and the Thiele modulus (Φ) for a first order reaction are given in equations (4) and (5), respectively.

$$\eta = \frac{\tanh(\Phi)}{\Phi} \tag{4}$$

$$\Phi^2 = \frac{a_c \cdot m_{Pd} \cdot L^2_{cat}}{V_{cat} \cdot D_E \cdot C^{s}_{H_2}} \tag{5}$$

where a_c, L_{cat}, V_{cat}, and D_E refer to the intrinsic activity, the catalyst layer thickness, the catalyst volume, and the effective diffusivity, respectively. According to Meille et al. (Meille et al., 2002), the intrinsic activity can be obtained by equation (6).

$$a_c = k_0 \cdot \exp\left(-\frac{E_a}{RT}\right) \cdot \frac{k_{H_2} \cdot C^{l}_{H_2}}{\left(1 + \sqrt{k_{H_2} \cdot C^{l}_{H_2}}\right)^2} \tag{6}$$

where k_0, E_a, R, k_{H_2}, and $C^{l}_{H_2}$ refer to the Arrhenius pre-exponential factor, the activation energy, the gas constant, the hydrogen adsorption equilibrium constant, and the hydrogen concentration in the liquid, respectively. The equation (6) was chosen because the hydrogenation conditions (30 °C and 0.6 MPa) were similar as those in the literature (Meille et al., 2002), and referring to the estimated kinetic parameters by Meille et al., k_0 = 8.5 × 10^6 mol·s^{-1}·g^{-1}_{Pd}, E_a = 38.7 × 10^3 J·mol^{-1}, and k_{H_2} = 1.4 × 10^{-2} m^3·mol^{-1}. The unknown parameters in equations (1)–(6) were $C^{s}_{H_2}$, η, and Φ, which can be easily calculated to obtain k_{OV}.

3. Results and discussion

3.1. Characterization of catalysts

3.1.1. Coating weight

The coatings were prepared by slurry circulation method, and the effect of slurry flow rate on the coating weight of Al_2O_3, SiO_2, CeO_2, TiO_2, and $CaCO_3$ is shown in Fig. 3. The coating weight decreased with the increase of slurry flow rate, ranging from 0.18 to 0.06 g·(g nickel foam)$^{-1}$ for Al_2O_3, 0.13 to 0.04 g·(g nickel foam)$^{-1}$ for SiO_2, 2.23 to 0.60 g·(g nickel foam)$^{-1}$ for CeO_2, 0.39 to 0.13 g·(g nickel foam)$^{-1}$ for TiO_2, and 0.15 to 0.05 g·(g nickel foam)$^{-1}$ for $CaCO_3$. This is because the slurry in the pores of nickel foams flowed out with the air circulation, and more slurry can be removed by increasing the flow rate. In addition, the coating weight was affected by the density of powders and the viscosity of slurry.

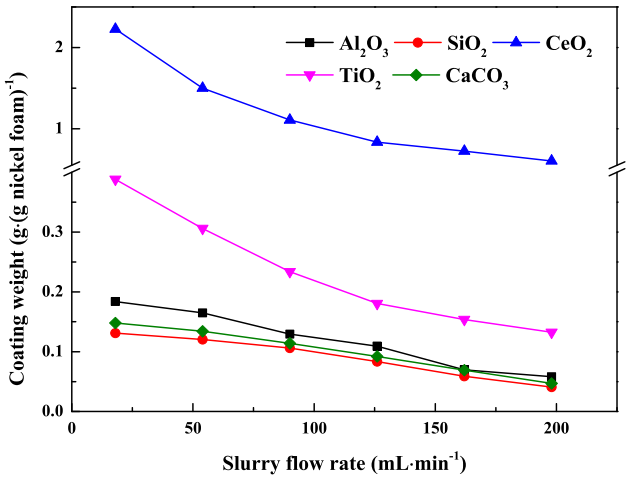

Fig. 3. Effect of slurry flow rate on coating weight.

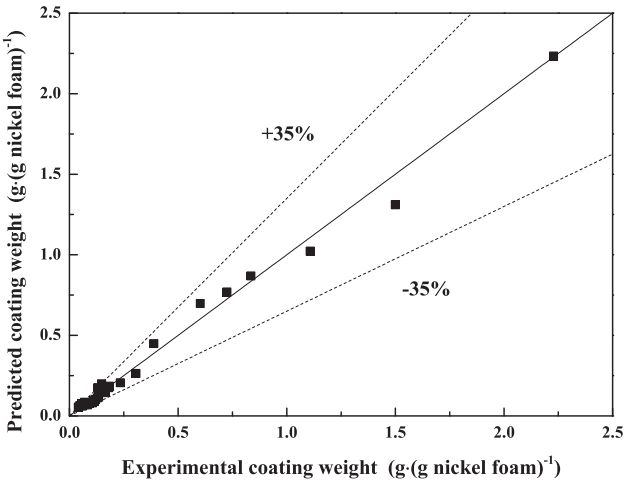

Fig. 4. Comparison of coating weight between predicted and experimental values.

An empirical correlation of the coating weight on the nickel foams, considering slurry flow rate, density of powders (ρ) and viscosity of slurry (μ) was proposed to evaluate their contribution. The density of Al_2O_3, SiO_2, CeO_2, TiO_2, and $CaCO_3$ powders and the viscosity of corresponding slurry are listed in Table 1, and the correlation is expressed as follows:

$$m = 0.0852 \times Q_s^{-0.49} \times \rho^{2.97} \times \mu^{-0.84} \quad (R^2 = 0.9726) \tag{7}$$

The predicted values agreed well with the experimental values with the errors of ±35%, as shown in Fig. 4, indicating the practicality of this correlation to predict the coating weight. According to the results in Fig. 3, the correlation was applicable with the coating weight of 0.04 to 2.23 g·(g nickel foam)$^{-1}$. The coating weight was proportional to the density's power of 2.97, and inversely proportional to the viscosity's power of 0.84 and to the flow rate's power of 0.49. When the density of powders was high, the weight of the remaining slurry with similar volume was large. The binding force between the powders was better than that between the powders and the nickel foam. Consequently, more slurry was removed by the air circulation when the viscosity was higher. The higher the flow rate, the stronger the slurry turbulence, the larger the air pressure, and the smaller the coating weight. This method can be used for coating various supports on the nickel foams with high applicability and accuracy. The experimental conditions can be calculated, and the required coating weight can be controlled according to the correlation.

3.1.2. Surface morphology

Fig. 5 displays the SEM micrographs of Al_2O_3 particle, nickel foam, pretreated nickel foam, and the coatings on nickel foams. The surface of nickel foam was flat and smooth, as shown in Fig. 5(b). After pretreatment, there were some pores formed on the surface of the nickel foam, as shown in Fig. 5(c). The roughness of the surface was improved by pretreatment, which was beneficial to the enhancement of the mechanical stability of coatings (Ma et al., 2019; Zhang et al., 2015). From Fig. 5(d), (e), (f), (g), and (h), it can be seen that the surface was further rough and irregular by coating the supports. At the slurry flow rate of 162 mL·min^{-1}, the Al_2O_3, SiO_2, CeO_2, TiO_2, and $CaCO_3$ coatings were all uniform. When the slurry flow rate was increased or decreased, the coatings remained uniform except for $CaCO_3$ at low flow rate of 54 mL·min^{-1}, as displayed in Fig. S.1. The main reason is that the agglomeration of $CaCO_3$ particles occurred at low flow rate, and the agglomeration was eliminated with the strong turbulence of slurry at high flow rate. As shown in Fig. 5(d) and (g), and Fig. S.1 (a1), (a2), and (d2), the Al_2O_3 and TiO_2 coatings had pore structures because of the high viscosity of slurry. The bubbles were generated and mixed in the slurry when the slurry was circulated through the pores of the nickel foams.

The surface of Al_2O_3 particle was also rough with blocky structures. Conversely, the surface of Al_2O_3 particle was less uniform than that of the monolithic catalyst coatings. Most of the coatings prepared by slurry circulation are uniform, especially at high flow rate, which is beneficial to the improvement of the uniformity of active components and the performance of catalysts.

Whereafter, the coatings with the slurry flow rate of 162 mL·min^{-1} were chosen as examples for loading active component Pd. Fig. 6 presents the SEM micrographs of Pd/Al_2O_3 catalyst particle, Pd/Al_2O_3, Pd/SiO_2, Pd/CeO_2, Pd/TiO_2, and Pd/$CaCO_3$ catalyst coatings on the nickel foams. It is obvious that the surfaces of catalyst coatings were all uniform, and the surface of Pd/Al_2O_3 catalyst particle was nonuniform, which were consistent with the corresponding supports. This suggested that the loading process of active components had little influence on the morphologies of the Al_2O_3 particles and the coatings.

The large range of coatings and the loading effects can be observed from the SEM micrographs with low magnification (×100), as shown in Fig. S.2. The catalyst coatings were uniform, and the pores of nickel foams were not blocked by the coatings. The preparation method of catalysts may have the advantages in overcoming capillary force and intensifying reaction process.

Table 1
Density of support powders and viscosity of corresponding slurry.

Support	Powders density (g·cm^{-3})	Slurry viscosity (cP)
Al_2O_3	3.7	5.46
SiO_2	2.2	1.29
CeO_2	7.1	3.93
TiO_2	4.3	4.51
$CaCO_3$	2.9	2.95

3.1.3. Textural property

The textural properties of Al_2O_3 particles, nickel foam, pretreated nickel foam, Al_2O_3, SiO_2, CeO_2, TiO_2, and $CaCO_3$ coatings on nickel foams, and the corresponding catalyst coatings on nickel foams are summarized in Table 2. The specific surface area, pore volume, and average pore size of pretreated nickel foam were larger than those of original nickel foam by reason of the formation of pore structures during the pretreatment. After coated with Al_2O_3,

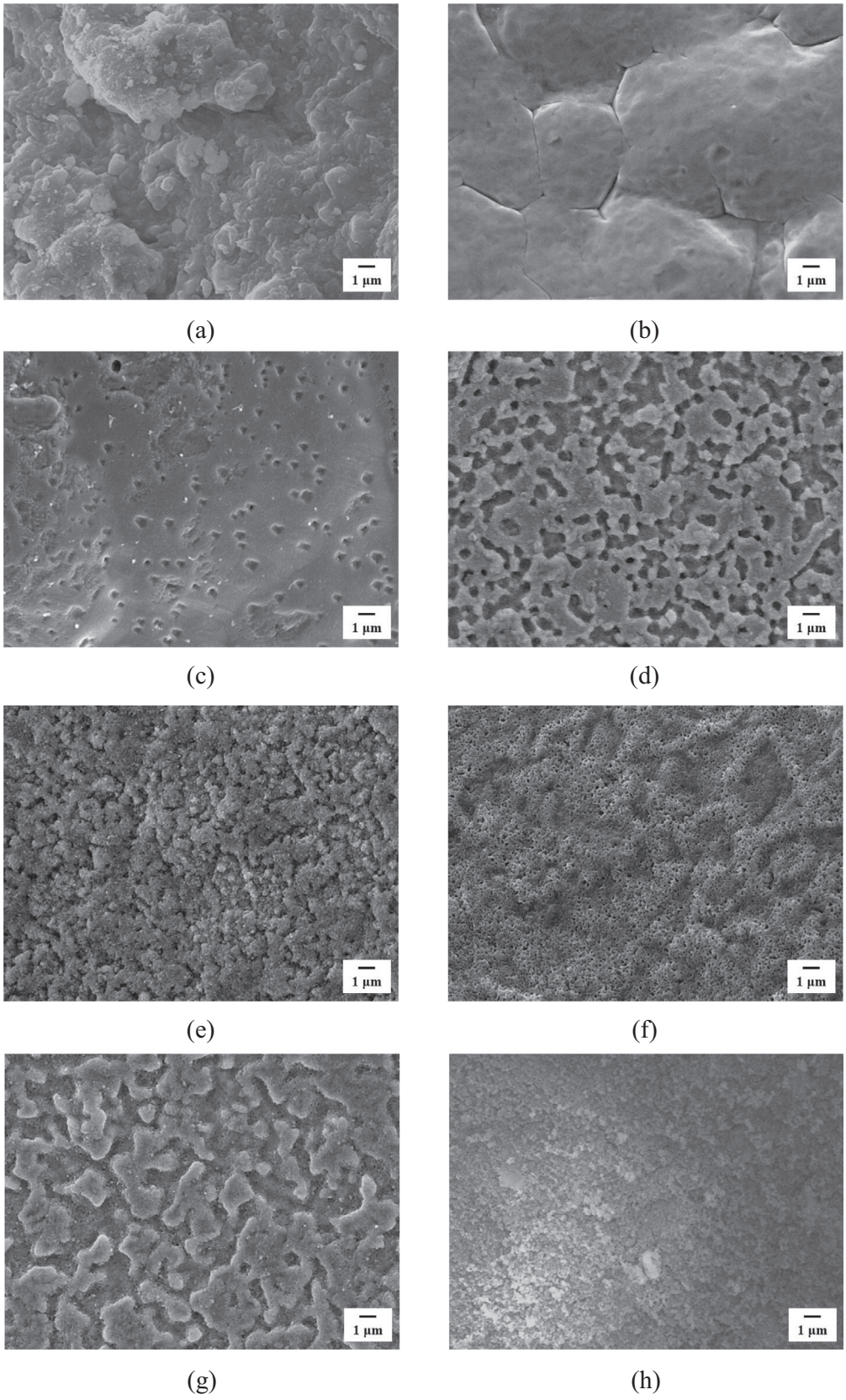

Fig. 5. SEM micrographs of (a) Al_2O_3 particle, (b) nickel foam, (c) pretreated nickel foam, (d) Al_2O_3, (e) SiO_2, (f) CeO_2, (g) TiO_2, and (h) $CaCO_3$ coatings on nickel foams with slurry flow rate of 162 mL·min^{-1}.

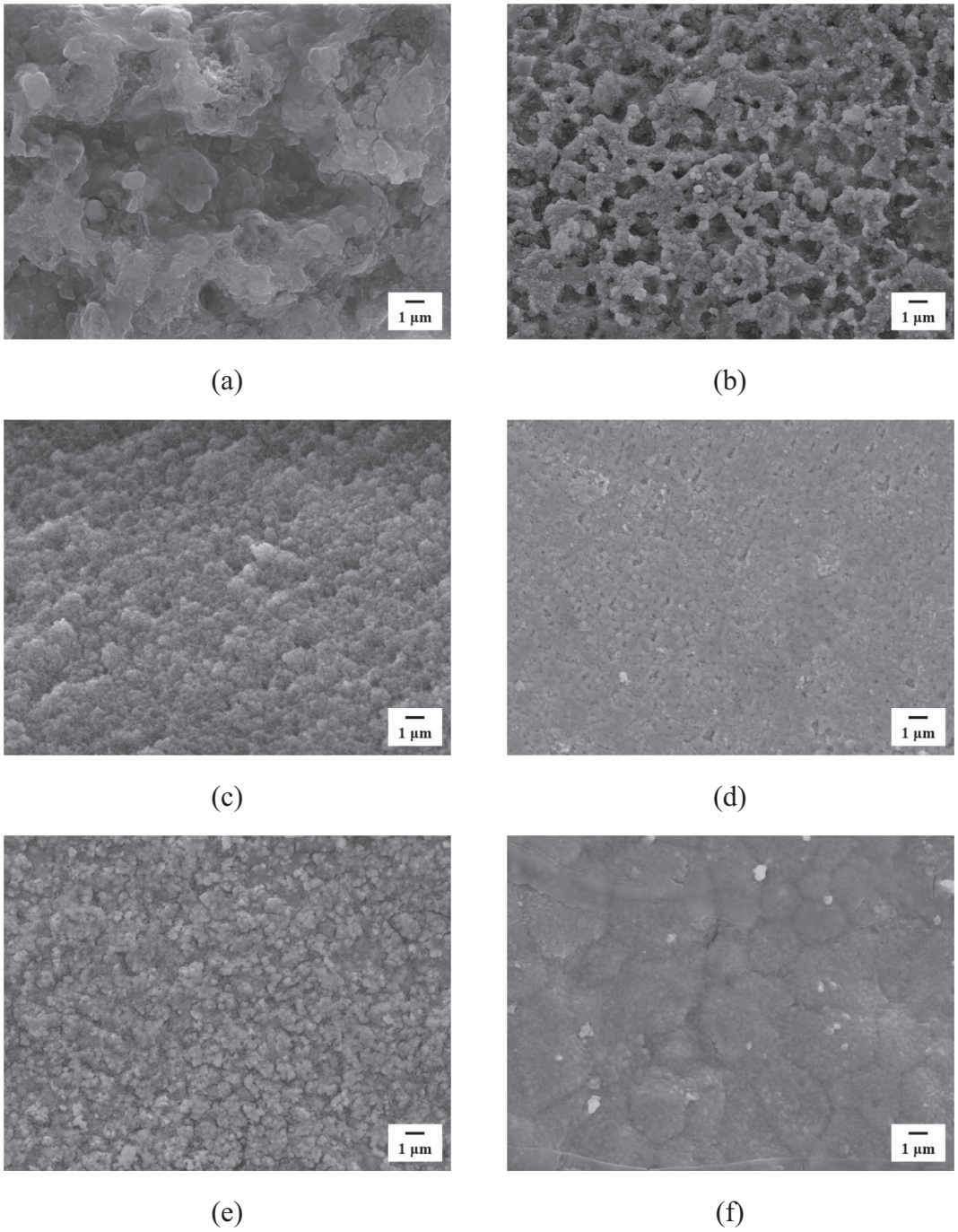

Fig. 6. SEM micrographs of (a) Pd/Al_2O_3 particle, (b) Pd/Al_2O_3, (c) Pd/SiO_2, (d) Pd/CeO_2, (e) Pd/TiO_2, and (f) $Pd/CaCO_3$ coatings on nickel foams.

SiO_2, CeO_2, TiO_2, and $CaCO_3$, the specific surface areas of pretreated nickel foams increased, and the order of specific surface area was $SiO_2 > Al_2O_3 > CeO_2 > CaCO_3 > TiO_2$, which was mainly related to the specific surface area of the powders. The pore volumes of the coatings on nickel foams also increased except for $CaCO_3$, and the average pore sizes decreased. This is because the powders have abundant pore structures, and compared with the pretreated nickel foams, the powders have larger pore volumes and smaller average pore sizes. While the pore volume of $CaCO_3$ was smaller than that of pretreated nickel foams. In general, slurry circulation can be a practical method for preparing coatings on the nickel foams with different kinds of supports and different coating weights, which is consistent with the analysis results of the correlation and surface morphologies.

The specific surface areas of nickel foams further increased, and the pore volumes and the average pore sizes decreased with the loading of active component Pd. The main reason is that Pd small particles were deposited on the surface of coatings and also accessed into the pores. The loading process of active components did not significantly affect the textural properties of the coatings. The variation tendency for the specific surface area, pore volume, and average pore size of Al_2O_3 particles is the same as that for nickel foams with the similar reasons. Compared with the particle catalysts, the monolithic catalysts had the smaller specific surface

Table 2
Textural properties of Al_2O_3 particles, nickel foam, pretreated nickel foam, support coatings, and corresponding catalyst coatings on nickel foams.

Parameter	Surface area ($m^2 \cdot g^{-1}$)	Pore volume ($cm^3 \cdot g^{-1}$)	Pore size (nm)
Al_2O_3 particles	191.8	0.7750	16.2
Pd/Al_2O_3 particles	203.1	0.7590	15.0
Nickel foam	10.4	0.0610	23.4
Pretreated nickel foam	15.3	0.1173	39.3
Al_2O_3 coatings	47.8	0.2038	17.1
Pd/Al_2O_3 coatings	47.9	0.1545	8.9
SiO_2 coatings	55.2	0.1933	14.0
Pd/SiO_2 coatings	57.5	0.1774	7.1
CeO_2 coatings	29.0	0.1647	22.7
Pd/CeO_2 coatings	31.3	0.1102	14.4
TiO_2 coatings	16.0	0.1919	5.4
Pd/TiO_2 coatings	19.6	0.1448	5.3
$CaCO_3$ coatings	24.8	0.0926	17.0
$Pd/CaCO_3$ coatings	26.6	0.0747	14.5

area and pore volume, because the nickel foam substrate occupied most of the mass.

3.2. Hydrogenation performance of catalysts

3.2.1. Catalyst activity

The hydrogenation reaction was performed in the MPB with the similar Pd content of about 0.00012 g for both particle catalysts and monolithic catalysts. The effect of liquid flow rate on the activity of particle catalysts and monolithic catalysts is shown in Fig. 7. The AMS conversion decreased with the increase of liquid flow rate. Although the increase of liquid flow rate may improve the mass transfer efficiency, AMS cannot contact adequately with Pd sites and flows directly through the reactor at high liquid flow rate. With increasing the liquid flow rate, the residence time of liquid reactant decreased. The decreasing tendency of conversion at high liquid flow rate was not significant than that at low liquid flow rate. Comparing the activity of the monolithic catalysts with the same content of Pd, the catalysts with Pd/CeO_2 and $Pd/CaCO_3$ coatings had the highest and lowest AMS conversion, respectively. The catalysts with Pd/Al_2O_3, Pd/SiO_2, and Pd/TiO_2 coatings had little difference in AMS conversion. The possible reason is that there was difference in the textural properties between the coatings, and the capabilities of the coatings for the combination and storage of gas and liquid reactants were also different. Besides, the uniformity of active component Pd dispersed on the coatings can also affect the catalyst activity.

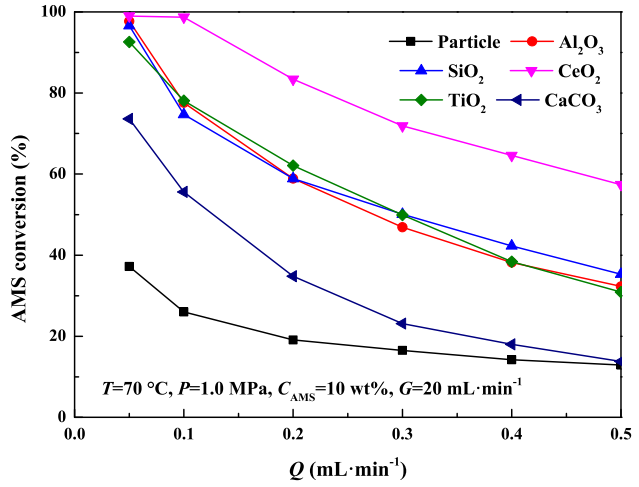

Fig. 7. Effect of liquid flow rate on catalyst activity in the MPB.

For the investigation of the uniformity, the Pd distribution on the coatings was analyzed through the EDS mapping images, as shown in Fig. 8, which are corresponding to the SEM micrographs in Fig. 6. It can be seen that the Pd dispersed on Al_2O_3, SiO_2, CeO_2, TiO_2, and $CaCO_3$ coatings was uniform. This indicated that the coatings prepared by slurry circulation can promote the uniformity of Pd distribution because of the uniform distribution of the coatings. Therefore, Pd distribution may have little effect on the catalyst activity, and the difference in catalyst activity mainly depend on the properties of coatings.

The monolithic catalysts had the higher AMS conversion compared with the particle catalysts, as shown in Fig. 7. At the liquid flow rate of 0.05 $mL \cdot min^{-1}$, the AMS conversion of Pd/Al_2O_3/nickel foam and Pd/Al_2O_3 particle catalysts had the maximum difference as 60.5%. The Pd distribution on the particle catalysts was also uniform, as shown in Fig. 8(a). Although the particles had the higher Al_2O_3 content and the larger specific surface area, there was higher internal mass transfer resistance inside the catalysts, and it is more difficult for the reactants to reach the Pd sites in the particles. This suggested that the thin layer of Al_2O_3 coatings on nickel foams had significant advantages for the improvement of active component utilization and internal mass transfer.

3.2.2. Catalyst stability

The catalyst stability is one of the important parameters for catalytic reactions, so the long-term stability and the mechanical stability were investigated in this work. Fig. 9 displays the activity of particle catalysts and monolithic catalysts in the MPB for 72 h. Obviously, the stabilities of all catalysts were fairly high. The activity of the monolithic catalysts with Al_2O_3 and SiO_2 coatings slightly decreased in the first 16 h because of a small loss of catalyst coatings. Subsequently, the activity remained stable for a period of 56 h. In contrast, the activity of the particle catalysts and the monolithic catalysts with CeO_2, TiO_2, and $CaCO_3$ coatings slowly decreased in 72 h. The possible reason is that the mass loss of particles and coatings occurred during the gas and liquid scouring. The decrease of AMS conversion for the particle catalysts and the monolithic catalysts with Al_2O_3, SiO_2, CeO_2, TiO_2, and $CaCO_3$ coatings was 1.5%, 4.8%, 3.0%, 6.0%, 7.0%, and 6.2%, respectively. Compared with the monolithic catalysts, the particle catalysts had relatively higher stability because the adhesion between Al_2O_3 was stronger than that between Al_2O_3 and nickel foam. Compared with nickel foam, Al_2O_3 particles have more rough structures on the surface and between the particles. Other Al_2O_3 particles diffused into these structures, which can provide mechanical adhesion. In addition, the surface of Al_2O_3 particles adsorbed more polar groups than that of nickel foam, promoting the formation of more chemical bonds between Al_2O_3 particles to improve adhesion. These are beneficial to the improvement of stability. Among the monolithic catalysts, Pd/SiO_2/nickel foam catalysts demonstrated the highest stability by reason of the strongest adhesion.

After the long-term experiments, the catalysts were washed and dried, and the mass loss before and after the experiments was measured to evaluate the mechanical stability. The mass losses of the particle catalysts and the monolithic catalysts with Al_2O_3, SiO_2, CeO_2, TiO_2, and $CaCO_3$ coatings were 1.6%, 3.2%, 2.4%, 5.6%, 8.1%, and 6.3%, respectively. The order of mechanical stability was quite consistent with that of long-term stability. This verified that the decrease in activity mainly resulted from the loss of particles and coatings. The method of slurry circulation for preparing monolithic catalysts can provide high activity and stability during the hydrogenation reaction.

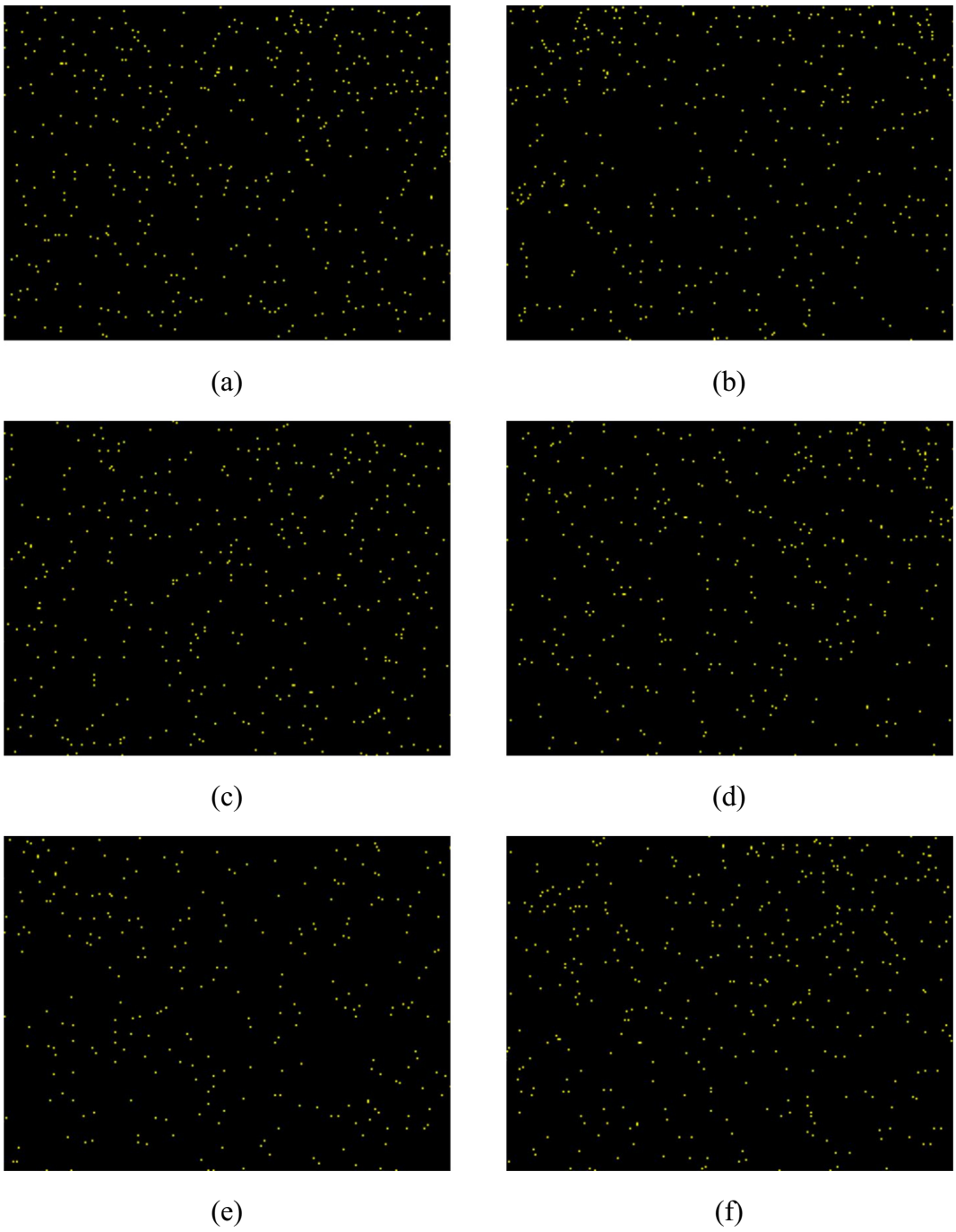

Fig. 8. EDS mapping images of Pd distribution on (a) Al_2O_3 particle, (b) Al_2O_3, (c) SiO_2, (d) CeO_2, (e) TiO_2, and (f) $CaCO_3$ coatings.

3.3. Mass transfer performance of catalysts

3.3.1. Overall external mass transfer performance

Fig. 10 shows the effect of liquid superficial velocity on the overall external mass transfer coefficient of the MPB with particle catalysts and monolithic catalysts. The k_{OV} increased with the increase of liquid superficial velocity, because the liquid turbulence and liquid renewal rate were enhanced at high liquid superficial velocity. This can lead to the improvement of gas–liquid and liquid–solid contact areas and the intensification of gas–liquid and liquid–solid mass transfer processes.

The difference of k_{OV} between the monolithic catalysts was not significant. This is because the liquid flow and liquid contact states were similar on the coatings with the same pore size of nickel foam in the same MPB. The order of k_{OV} was similar to that of the catalyst activity, indicating that the coatings had a certain influence on k_{OV}, and the difference mainly attributed to the catalyst properties. The k_{OV} of particle catalysts was higher than that of monolithic catalysts, which was contrary to the tendency of catalyst activity. The reason is that the porosity of particle catalysts was lower than that of monolithic catalysts, and it is easier for the liquid to contact with the Pd sites on particle catalysts, which improved the liquid–solid

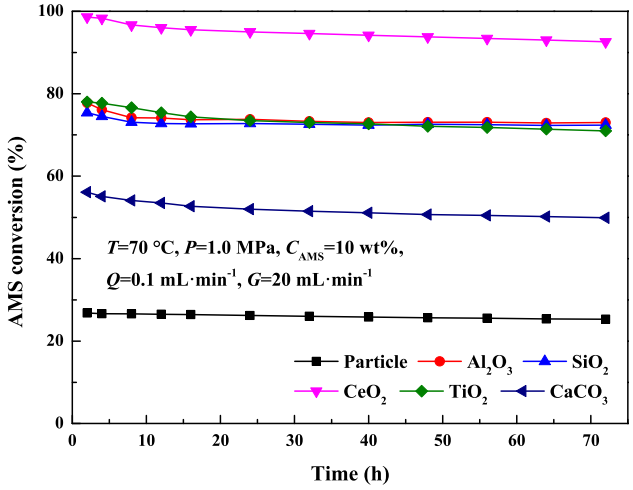

Fig. 9. Long-term stability of catalysts in the MPB.

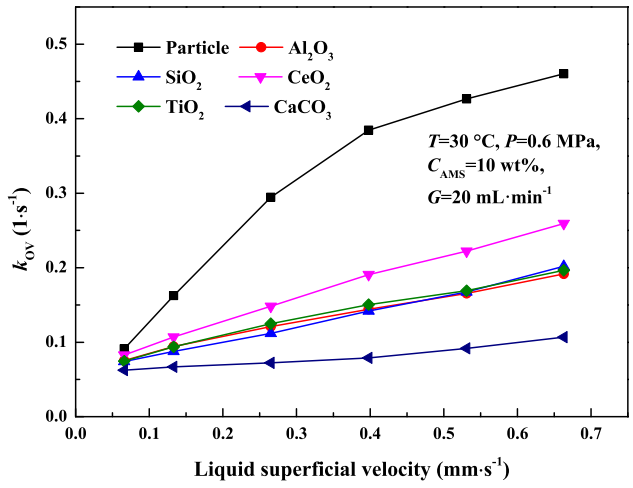

Fig. 10. Effect of liquid superficial velocity on k_{OV} of MPB with particle and monolithic catalysts.

mass transfer performance. However, the activity of monolithic catalysts was relatively high because of the small internal mass transfer limitation, as described in Section 3.2.1. This suggested that the hydrogenation in monolithic catalysts was mainly controlled by external mass transfer process.

3.3.2. Correlation of mass transfer coefficients

An attempt of overall external mass transfer coefficient modelling was proposed. To predict the k_{OV} of the MPB with monolithic catalysts, dimensionless numbers including liquid Reynolds number (Re_l), gas Reynolds number (Re_g), and liquid Schmidt number (Sc_l) were used (Lévêque et al., 2016; Tourvieille et al., 2015; Haase et al., 2013; Sang et al., 2020), and the coating weight (W) and the specific surface area (S), which may affect the overall external mass transfer performance were also taken into account. Fig. S.3 shows the effect of gas superficial velocity on k_{OV} of the MPB with Pd/Al_2O_3/nickel foam catalysts, and the dimensionless numbers were calculated based on the data in Fig. 10 and Fig. S.3. The correlation is shown below:

$$\frac{k_{OV}\cdot d_p^2}{D_{H_2}^l} = 0.0137 \times Re_l^{0.46} \times Re_g^{-0.05} \times Sc_l^{0.33} \times W^{0.13} \times S^{0.07} \quad (R^2 = 0.9527) \tag{8}$$

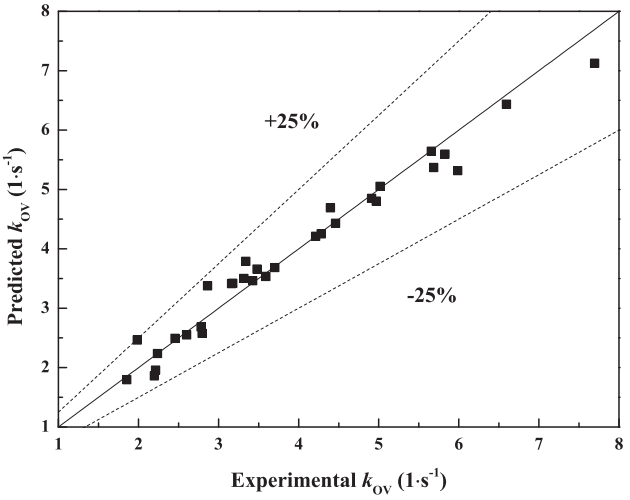

Fig. 11. Comparison of k_{OV} between predicted and experimental values.

where d_p and $D_{H_2}^l$ refer to the pore size of nickel foam and the molecular diffusivity in the liquid phase, respectively. The correlation was applicable when the k_{OV} was between 0.0625 and 0.2594 s^{-1}. According to the experimental data, the ranges of application for W and S were from 0.06 to 0.72 g·(g nickel foam)$^{-1}$ and 19.6 to 57.5 $m^2 \cdot g^{-1}$, respectively. Sc_l is constant (Lévêque et al., 2016; Tourvieille et al., 2015; Haase et al., 2013; Sang et al., 2020), and Re_l, Re_g, W, and S all had a certain influence on k_{OV}. The influence of Re_l and Re_g was the largest and smallest, respectively. As shown in Fig. 11, the relative errors between predicted values and experimental values were almost within ±25%. This suggested that there was a good practicality for the correlation to predict the k_{OV} of the MPB with monolithic catalysts.

4. Conclusions

In this work, a universal and applicable method of slurry circulation was proposed to prepare monolithic catalysts used in MPBs. Al_2O_3, SiO_2, CeO_2, TiO_2, and $CaCO_3$ were coated on the nickel foams with good uniformity, and the coating weight can be controlled by empirical correlation. The Pd was also uniformly distributed on the coatings. During the AMS hydrogenation process in the MPB, the monolithic catalysts exhibited the higher activity compared with the particle catalysts because of the high internal mass transfer performance. The stability of monolithic catalysts was high with a slight decrease in the first 16 h, resulting from the small loss of coatings. The k_{OV} of the MPB with monolithic catalysts was relatively low, indicating that the hydrogenation was mainly controlled by external mass transfer process. The correlation was proposed and the predicted k_{OV} agreed well with the experimental k_{OV}. The catalysts prepared by slurry circulation with uniform support coatings and active components hopefully provide high activity and stability in MPBs.

CRediT authorship contribution statement

Chi Ma: Investigation, Software, Writing – original draft, Writing – review & editing. **Mengmeng Huang:** Investigation, Writing – review & editing. **Jiabin Yin:** Software. **Fengyan Lou:** Investigation. **Jisong Zhang:** Investigation, Writing – review & editing, Funding acquisition.

Declaration of Competing Interest

The authors declare that they have no known competing financial interests or personal relationships that could have appeared to influence the work reported in this paper.

Acknowledgements

We gratefully acknowledge the supports of National Natural Science Foundation of China (22022809, 22008138, and 21991103) on this work.

Appendix A. Supplementary material

Supplementary data to this article can be found online at https://doi.org/10.1016/j.ces.2022.117477.

References

Bobadilla, L.F., Alvarez, A., Dominguez, M.I., Romero-Sarria, F., Centeno, M.A., Montes, M., Odriozola, J.A., 2012. Influence of the shape of Ni catalysts in the glycerol steam reforming. Appl. Catal., B 123, 379–390.

Cao, Q., Sang, L., Tu, J.C., Xiao, Y.S., Liu, N., Wu, L.D., Zhang, J.S., 2021. Rapid degradation of refractory organic pollutants by continuous ozonation in a micro-packed bed reactor. Chemosphere 270, 128621.

Chen, X., Li, J.Y., Wang, Y., Zhou, Y., Zhu, Q.L., Lu, H.F., 2020. Preparation of nickel-foam-supported Pd/NiO monolithic catalyst and construction of novel electric heating reactor for catalytic combustion of VOCs. Appl. Catal., A 607, 117839.

Feng, H., Zhu, X., Chen, R., Liao, Q., Liu, J., Li, L., 2016. High-performance gas-liquid-solid microreactor with polydopamine functionalized surface coated by Pd nanocatalyst for nitrobenzene hydrogenation. Chem. Eng. J. 306, 1017–1025.

Haase, S., Weiss, M., Langsch, R., Bauer, T., Lange, R., 2013. Hydrodynamics and mass transfer in three-phase composite minichannel fixed-bed reactors. Chem. Eng. Sci. 94, 224–236.

Herskowitz, M., Morita, S., Smith, J.M., 1978. Solubility of hydrogen in α-methylstyrene. J. Chem. Eng. Data 23, 227–228.

Jin, J.K., Kwon, S.J., 2009. Microcatalytic combustion of H_2 on Pt/Al_2O_3-coated nickel foam. Combust. Sci. Technol. 181 (2), 211–225.

Kataoka, S., Takeuchi, Y., Harada, A., Takagi, T., Takenaka, Y., Fukaya, N., Yasuda, H., Ohmori, T., Endo, A., 2012. Microreactor containing platinum nanoparticles for nitrobenzene hydrogenation. Appl. Catal., A 427, 119–124.

Koc, S., Avci, A.K., 2017. Reforming of glycerol to hydrogen over Ni-based catalysts in a microchannel reactor. Fuel Process. Technol. 156, 357–365.

Lévêque, J., Philippe, R., Zanota, M.L., Meille, V., Sarrazin, F., Baussaron, L., de Bellefon, C., 2016. Hydrodynamics and mass transfer in a tubular reactor containing foam packings for intensification of G-L-S catalytic reactions in co-current up-flow configuration. Chem. Eng. Res. Des. 109, 686–697.

Li, Y.H., Zhu, L.H., Yan, K.Q., Zheng, J.B., Chen, B.H., Wang, W.J., 2013. A novel modification method for nickel foam support and synthesis of a metal-supported hierarchical monolithic Ni@Pd catalyst for benzene hydrogenation. Chem. Eng. J. 226, 166–170.

Liang, Z.D., Gao, P., Tang, Z.Y., Lv, M., Sun, Y.H., 2017. Three dimensional porous Cu-Zn/Al foam monolithic catalyst for CO_2 hydrogenation to methanol in microreactor. J. CO2 Util. 21, 191–199.

Liu, M., Zhu, X., Chen, R., Liao, Q., Feng, H., Li, L., 2016. Catalytic membrane microreactor with $Pd/\gamma\text{-}Al_2O_3$ coated PDMS film modified by dopamine for hydrogenation of nitrobenzene. Chem. Eng. J. 301, 35–41.

Losey, M.W., Schmidt, M.A., Jensen, K.F., 2001. Microfabricated multiphase packed-bed reactors: characterization of mass transfer and reactions. Ind. Eng. Chem. Res. 40, 2555–2562.

Ma, C., Luo, Y., Sun, B.C., Su, M.J., Chu, G.W., Chen, J.F., 2019. Efficient coating method via matching rough surface of stainless steel with Al_2O_3 particles. Ind. Eng. Chem. Res. 58 (5), 1848–1856.

Ma, C., Duan, X.N., Yin, J.B., Sang, L., Zhang, J.S., 2021. Preparation of Pd/Al_2O_3/nickel microfoam catalysts by electrodeposition for hydrogenation in a micropacked bed reactor. Ind. Eng. Chem. Res. https://doi.org/10.1016/j.cjche.2021.05.022.

Meille, V., de Bellefon, C., Schweich, D., 2002. Kinetics of α-methylstyrene hydrogenation on Pd/Al_2O_3. Ind. Eng. Chem. Res. 41 (7), 1711–1715.

Meille, V., Pestre, N., Fongarland, P., de Bellefon, C., 2004. Gas/liquid mass transfer in small laboratory batch reactors: comparison of methods. Ind. Eng. Chem. Res. 43, 924–927.

Nuzhdin, A.L., Moroz, B.L., Bukhtiyarova, G.A., Reshetnikov, S.I., Pyrjaev, P.A., Aleksandrov, P.V., Bukhtiyarov, V.I., 2015. Selective liquid-phase hydrogenation of a nitro group in substituted nitrobenzenes over Au/Al_2O_3 catalyst in a packed-bed flow reactor. ChemPlusChem 80 (12), 1741–1749.

Ranade, V.V., Chaudhari, R.V., Gunjal, P.R., 2011. Trickle Bed Reactors: Reactor Engineering & Applications. Kidlington, Oxford, UK.

Roy, P.S., Song, J., Kim, K., Kim, J.M., Park, C.S., Raju, A.S.K., 2018. Effects of $CeZrO_2$-Al_2O_3 support composition of metal-foam-coated Pd-Rh catalysts for the steam-biogas reforming reaction. J. Ind. Eng. Chem. 62, 120–129.

Sang, L.X., Sun, B.A., Tan, H.Y., Du, C.X., Wu, Y.T., Ma, C.F., 2012. Catalytic reforming of methane with CO_2 over metal foam based monolithic catalysts. Int. J. Hydrogen Energ. 37 (17), 13037–13043.

Sang, L., Feng, X.D., Tu, J.C., Xie, B.Q., Luo, G.S., Zhang, J.S., 2020. Investigation of external mass transfer in micropacked bed reactors. Chem. Eng. J. 393, 124793.

Sang, L., Tu, J.C., Cheng, H., Luo, G.S., Zhang, J.S., 2020. Hydrodynamics and mass transfer of gas-liquid flow in micropacked bed reactors with metal foam packing. AIChE J. 66 (2), e16803.

Shang, M.J., Noel, T., Wang, Q., Hessel, V., 2013. Packed-bed microreactor for continuous-flow adipic acid synthesis from cyclohexene and hydrogen peroxide. Chem. Eng. Technol. 36, 1001–1009.

Shang, M.J., Noel, T., Wang, Q., Su, Y.H., Miyabayashi, K., Hessel, V., Hasebe, S., 2015. 2-and 3-Stage temperature ramping for the direct synthesis of adipic acid in micro-flow packed-bed reactors. Chem. Eng. J. 260, 454–462.

Sudhakaran, M.S.P., Hossain, M.M., Gnanasekaran, G., Mok, Y.S., 2019. Dry reforming of propane over $\gamma\text{-}Al_2O_3$ and nickel foam supported novel $SrNiO_3$ perovskite catalyst. Catalysts 9, 68.

Tourvieille, J.N., Bornette, F., Philippe, R., Vanderberghe, Q., de Bellefon, C., 2013. Mass transfer characterization of a microstructured falling film at pilot scale. Chem. Eng. J. 227, 182–190.

Tourvieille, J.N., Philippe, R., de Bellefon, C., 2015. Milli-channel with metal foams under an applied gas-liquid periodic flow: external mass transfer performance and pressure drop. Chem. Eng. J. 267, 332–346.

Tu, J.C., Sang, L., Cheng, H., Ai, N., Zhang, J.S., 2020. Continuous hydrogenolysis of *N*-diphenylmethyl groups in a micropacked-bed reactor. Org. Process Res. Dev. 24 (1), 59–66.

Vilé, G., Almora-Barrios, N., López, N., Pérez-Ramírez, J., 2015. Structure and reactivity of supported hybrid platinum nanoparticles for the flow hydrogenation of functionalized nitroaromatics. ACS Catal. 5 (6), 3767–3778.

Wang, F.H., Luo, Y.M., Wang, Y.A., Zhu, H., 2019. The preparation and performance of a novel spherical spider web-like structure Ru-Ni/Ni foam catalyst for $NaBH_4$ methanolysis. Int. J. Hydrogen Energ. 44 (26), 13185–13194.

Wang, C.X., Ping, D., Dong, X.F., Dong, Y.C., Zang, Y.H., 2016. Construction of Ru/Ni-Al-oxide/Ni-foam monolithic catalyst for deep-removing CO in hydrogen-rich gas via selective methanation. Fuel Process. Technol. 148, 367–371.

Xue, Y.E., Shao, P.H., Yuan, Y.X., Shi, W.X., Guo, Y., Zhang, B., Bao, X., Cui, F.Y., 2021. Monolithic nickel foam supported macro-catalyst: manipulation of charge transfer for enhancement of photo-activity. Chem. Eng. J. 418, 129456.

Yang, C.X., Teixeira, A.R., Shi, Y.X., Born, S.C., Lin, H.K., Song, Y.F.L., Martin, B., Schenkel, B., Lachegurabi, M.P., Jensen, K.F., 2018. Catalytic hydrogenation of *N*-4-nitrophenyl nicotinamide in a micro-packed bed reactor. Green Chem. 20 (4), 886–893.

Yu, H., Chen, H.Q., Pan, M.Q., Tang, Y., Zeng, K., Peng, F., Wang, H.J., 2007. Effect of the metal foam materials on the performance of methanol steam micro-reformer for fuel cells. Appl. Catal., A 327, 106–113.

Zanota, M.L., Pallier, S., Dousse, A., Lachambre, J., Meille, V., 2018. Demonstration of the use of 3D X-ray tomography to compare the uniformity of catalyst coatings in open-cell foams. ChemEngineering 2, 52.

Zhang, L., Ren, Y.L., Luo, Q., Ying, X., Xu, H., Xuan, J., 2015. A novel method to from well-adhered $\gamma\text{-}Al_2O_3$ coating in 316L stainless steel microchannels. Energ. Procedia 75, 2044–2048.

Zhang, J.S., Teixeira, A.R., Kogl, L.T., Yang, L., Jensen, K.F., 2017. Hydrodynamics of gas-liquid flow in micropacked beds: pressure drop, liquid holdup, and two-phase model. AIChE J. 63, 4694–4704.

Zhang, J.S., Teixeira, A.R., Jensen, K.F., 2018. Automated measurements of gas-liquid mass transfer in micropacked bed reactors. AIChE J. 64 (2), 564–570.

Zheng, T.Q., Zhou, W., Gao, Y., Yu, W., Liu, Y.X., Zhang, C.Y., Zheng, C.C., Wan, S.L., Lin, J.D., Xiang, J.H., 2019. Active impregnation method for copper foam as catalyst support for methanol steam reforming for hydrogen production. Ind. Eng. Chem. Res. 58 (11), 4387–4395.

Zhu, J., Cao, L.Q., Li, C.Y., Zhao, G.F., Zhu, T., Hu, W., Sun, W.D., Lu, Y., 2019. Nanoporous Ni_3P evolutionarily structured onto a Ni foam for highly selective hydrogenation of dimethyl oxalate to methyl glycolate. ACS Appl. Mat. Inter. 11 (41), 37635–37643.